Materials Research Bulletin 151 (2022) 111797

Contents lists available at ScienceDirect

Materials Research Bulletin

journal homepage: www.elsevier.com/locate/matresbu

Research Papers

Cr^{3+} and Nd^{3+} co-activated garnet phosphor for NIR super broadband pc-LED application

Shuai He [a,d], Liangliang Zhang [a,*], Jingnan Zhang [a,b], Zhendong Hao [a], Hao Wu [a], Huajun Wu [a], Yongshi Luo [a], Guohui Pan [a], Feng Liu [c], Jiahua Zhang [a,b]

[a] State Key Laboratory of Luminescence and Applications, Changchun Institute of Optics, Fine Mechanics and Physics, Chinese Academy of Sciences, 3888 Eastern South Lake Road, Changchun 130033, China
[b] Center of Materials Science and Optoelectronics Engineering, University of Chinese Academy of Sciences, Beijing 100049, China
[c] Key Laboratory for UV-Emitting Materials and Technology of Ministry of Education, Northeast Normal University, Changchun 130024, China
[d] School of Science, Inner Mongolia University of Science and Technology, Baotou 014010, China

ARTICLE INFO

Keywords:
Broadband NIR phosphor
NIR pc-LEDs
Spectral complementation

ABSTRACT

Near-infrared phosphor converted light emitting diodes (NIR pc-LEDs), as a compact light source, play a constructive role in wearable optical biosensing devices. In order to detect the properties of different substances, the NIR emission should be as wide as possible. The typical strategy for broadening the band is the superposition emission of Cr^{3+} and Yb^{3+}, the bandwidth of which is 300–320 nm, and it needs to be further broadened. In this paper, NIR $Ca_2LuZr_2Al_3O_{12}$ garnet phosphor, co-activated by Cr^{3+} and Nd^{3+}, is prepared. The emission quantum efficiencies of Nd^{3+} at 900 nm and 1060 nm are close to 100%, and the emission band is complementary to that of Yb^{3+} at 1030 nm. An efficient super broadband NIR pc-LEDs (47.6 mW@100 mA), with the bandwidth of 350 nm, are achieved. The bandwidth and the efficiency of the pc-LEDs are improved greatly, compared with other reported ones.

1. Introduction

Near-infrared (NIR) light source, with continuous emission in 700–1100 nm, is demanded by NIR spectroscopy, which can be applied in food analysis, bio-sensing and medicine [1–8]. Phosphor converted LED (pc-LED) is the most promising one in recent years. The broadband NIR pc-LED is fabricated by integrating the broadband NIR phosphor and blue LED chip. Thus, developing efficient broadband NIR phosphor is particularly important.

Many broadband NIR phosphors have been reported recently [9–31]. They are mainly Cr^{3+} singly doped materials, such as $Lu_3Al_5O_{12}$: Ce^{3+}, Cr^{3+}, [6] $ScBO_3$: Cr^{3+}, [7] $Ca_2LuZr_2Al_3O_{12}$: Cr^{3+}, [19] La_2MgZrO_6: Cr^{3+}, [20] $Ca_3Sc_2Si_3O_{12}$: Cr^{3+}, [21] $LiInSi_2O_6$: Cr^{3+} [22] and $ZnAl_2O_4$: Cr^{3+} [23]. In addition, Xia et al. developed Eu^{2+} activated $K_3LuSi_2O_7$ phosphor, which showed the emission at 740 nm and a bandwidth of 160 nm [24]. Singly doped phosphors generally showed a bandwidth less than 200 nm, which limited the development of NIR pc-LED applications.

To further broaden the NIR emission band, emitting centers co-doped phosphors were developed. $La_3Ga_5GeO_{14}$: Cr^{3+}, reported by Liu et al., showed a bandwidth of 330 nm, which was originated from two Cr^{3+} centers. The NIR output power was 18.2 mW at 350 mA drive current [25]. The NIR emission of $Ca_3Sc_2Si_3O_{12}$: Cr^{3+}, Ln^{3+} (Ln = Nd^{3+}, Yb^{3+}), reported by Yao et al., showed a bandwidth of 330 nm, contributed from the energy transfer from Cr^{3+} to Nd^{3+} and Cr^{3+} to Yb^{3+}. And the NIR output power was 14.6 mW at 100 mA, corresponding to 4.9% electricity-to-NIR efficiency [26]. Recently, NIR broadband pc-LED with a bandwidth of 210 nm was fabricated by Yao et al., using $LiScP_2O_7$: Cr^{3+}, Yb^{3+} phosphor. And 36 mW NIR output light with 12% electricity-to-NIR efficiency at 100 mA drive current was achieved [27]. Basore et al. fabricated NIR pc-LED using the blend of $Gd_3Sc_{1.5}Al_{0.5}Ga_3O_{12}$: Cr^{3+}, Yb^{3+} and $LiInSi_2O_6$: Cr^{3+} phosphors. The pc-LED offered a 300 nm NIR bandwidth, and 50 mW NIR output power with 17% electricity-to-NIR efficiency at 100 mA [28]. In our previous work, $Ca_2LuZr_2Al_3O_{12}$: Cr^{3+}, Yb^{3+} showed a bandwidth of 320 nm and NIR output light was 41.8 mW at 100 mA drive current, corresponding to 14.3% electricity-to-NIR efficiency [29]. To meet the further demand of applications, the NIR pc-LEDs with broader bandwidth and high electricity-to-NIR efficiency are urgently needed.

In this study, Cr^{3+} and Nd^{3+} co-activated $Ca_2LuZr_2Al_3O_{12}$ (CLZA) is fabricated via high temperature solid state reaction. Its emission

* Corresponding author.
E-mail addresses: zhangliangliang@ciomp.ac.cn (L. Zhang), zhangjh@ciomp.ac.cn (J. Zhang).

https://doi.org/10.1016/j.materresbull.2022.111797
Received 1 November 2021; Received in revised form 19 January 2022; Accepted 18 February 2022
Available online 19 February 2022

spectrum including a Cr^{3+} emission band, at 800 nm, and a group of Nd^{3+} emission lines, distributed in range of 870–1100 nm and excited by energy transfer (ET) from Cr^{3+} to Nd^{3+}. Optical properties and thermal stabilities of $Ca_2LuZr_2Al_3O_{12}$: Cr^{3+}, Nd^{3+} are analyzed. A widely distributed NIR emission with a bandwidth of 350 nm is achieved. The as fabricated pc-LED offers 22.3% electricity-to-NIR efficiency at 10 mA, and the efficiency decreases to 16.2% at 100 mA with 47.6 mW NIR output power. The research data indicates that optical performance has greatly improved, compared with ever reported ones.

2. Experiment

2.1. Materials and synthesis

Nd^{3+} and Cr^{3+} co-activated $Ca_2LuZr_2Al_3O_{12}$ phosphors are synthesized via the high-temperature solid state reaction. $CaCO_3$ (99.99%), Lu_2O_3 (99.9%), ZrO_2 (99.99%), Al_2O_3 (99.9%), Cr_2O_3 (99.99%), and Nd_2O_3 (99.9%) are used as raw materials. The accurately weighed mixtures are grinded and put into the tube furnace heating by 3 °C/min, and protected by 10%H_2/N_2 gas flow. At first, the temperature raised to 900 °C, maintaining 1 h, and then raised to 1600 °C, maintaining 4 h. The final products, some green powders, are acquired after cooling down to room temperature. The PC-LED is fabricated by 460 nm chip and the blend of two NIR phosphor. The $Ca_2LuZr_2Al_3O_{12}$:8%Cr^{3+}, 2% Nd^{3+} phosphors, $Ca_2LuZr_2Al_3O_{12}$:8%Cr^{3+}, 2%Yb^{3+} phosphors and epoxide resin were fully mixed with 1:1:2 weigh ratio, then put it on the 460 nm chip, and then solidified at 200 °C for 20 min.

2.2. Characterization

The crystal pattern of $Ca_2LuZr_2Al_3O_{12}$ is detected by X-ray diffraction (XRD) (Bruker D8 Focus diffract meter, in the 2θ range from 15° to 75° with Cu Kα radiation (λ=1.54056 Å) operating at 40 kV, 30 mA); Photoluminescence excitation spectra are measured by FLS900 spectrometer (Edinburgh Instruments, U.K.); Photoluminescence spectra and the temperature-dependent properties are measured by HAAS2000 photoelectric spectrometer (350–1100 nm, EVERFINE, China), equipped with an excitation source (a 455 nm laser diode (LD)) and a THMS600E cooling-heating platform (77–873 K, Linkam Scientific Instruments, UK); The emission lifetime of Cr^{3+} and Nd^{3+} are measured by TRIAX 550 spectrometer, a pulsed laser as an excitation source; The photoelectric properties of the pc-LEDs are measured by HAAS2000 photoelectric measuring system (350–1100 nm, EVERFINE, China); The internal quantum efficiency (IQE) is measured using an absolute photoluminescence quantum yield measurement system (Quantaurus-QY Plus C13534–12, Hamamatsu Photonics).

3. Results and discussion

3.1. XRD patterns and crystal structure

The XRD patterns of $Ca_2LuZr_2Al_3O_{12}$:Cr^{3+}, xNd^{3+} (x = 0–8%) are shown in Fig. 1a. The XRD peaks shift to the left as the increase of x. This is because Nd^{3+} has replaced Lu^{3+} in $Ca_2LuZr_2Al_3O_{12}$:Cr^{3+}, Nd^{3+}, and the radius of Nd^{3+} (1.109 Å) is larger than that of Lu^{3+}(0.977 Å) [32]. A weak XRD peak (asterisk) of ZrO_2 is also detected at around 30°. Previous studies show that Cr^{3+} does not emit in ZrO_2 [19, 29]. Thus, the influence of ZrO_2 on luminescent properties of $Ca_2LuZr_2Al_3O_{12}$:Cr^{3+}, Nd^{3+} can be ignored. The crystal structure diagram of $Ca_2LuZr_2Al_3O_{12}$ and coordinate environments of Ca^{2+}/Lu^{3+}, Zr^{4+} and Al^{3+} are shown in Fig. 1b. The crystal structure of $Ca_2LuZr_2Al_3O_{12}$ is a garnet, as shown. The Ca^{2+}/Lu^{3+} connects with 8 oxygen atoms to form a [CaO_8] polyhedron. Zr^{4+} forms a [ZrO_6] octahedron. Al^{3+} forms a [AlO_4] tetrahedron.

3.2. Luminescence properties and energy transfer

The excitation and emission spectra of $Ca_2LuZr_2Al_3O_{12}$: 8% Cr^{3+}, monitored at 800 nm, are showed in Fig. 2a. From the picture, three excitation bands, at 300 nm, 460 nm and 640 nm, can be observed, which are assigned to $^4A_{2g}$→$^4T_{1g}$ (from ^4P orbit), $^4A_{2g}$→$^4T_{1g}$ (from ^4F) and $^4A_{2g}$→$^4T_{2g}$ (from ^4F) transitions of Cr^{3+}, respectively [29]. The weak excitation peak at 698 nm is originated from $^4A_{2g}$→^2E_g transition. The emission spectrum of $Ca_2LuZr_2Al_3O_{12}$: 8%Cr^{3+} shows a broadband at 800 nm, originated from $^4T_{2g}$(^4F) →$^4A_{2g}$ transition of Cr^{3+}. The excitation and emission spectra of $Ca_2LuZr_2Al_3O_{12}$: 4%Nd^{3+} can be found in Fig. 2b, in which a group of emission lines are observed. The line of 850–950 nm is originated from $^4F_{3/2}$→$^4I_{9/2}$ transition of Nd^{3+}, 1050–1150 nm is $^4F_{3/2}$ →$^4I_{11/2}$ and 1300–1450 nm is $^4F_{3/2}$ →$^4I_{13/2}$ [33–35]. The excitation spectrum of Nd^{3+} shows series lines, which are originated from transitions of Nd^{3+}, from $^4I_{9/2}$ to the $^4F_{3/2}$ or upper energy levels. The overlap of Nd^{3+}excitation peaks and the Cr^{3+}emission band indicates the possibility of energy transfer from Cr^{3+} to Nd^{3+}. The excitation spectrum of Cr^{3+} and Nd^{3+} co-doped $Ca_2LuZr_2Al_3O_{12}$ are shown in Fig. 2c and the energy transfer process is more evident, as shown. Moreover, the diffuse reflection spectra of the $Ca_2LuZr_2Al_3O_{12}$:

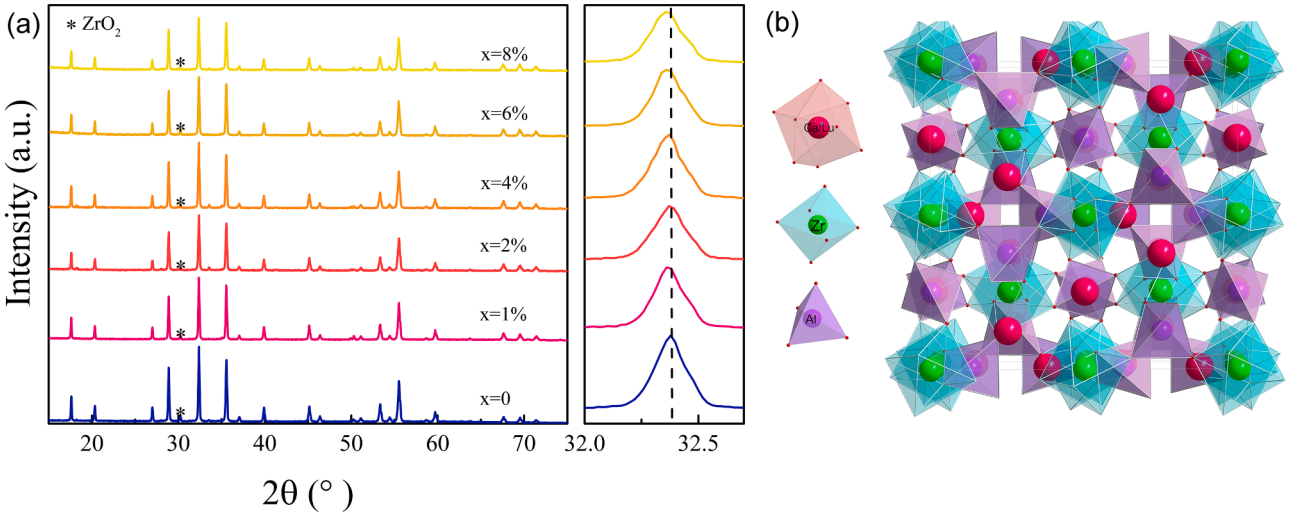

Fig. 1. XRD patterns of $Ca_2LuZr_2Al_3O_{12}$:8%Cr^{3+}, xNd^{3+} (x = 0–8%) (a) and structure diagram of $Ca_2LuZr_2Al_3O_{12}$ and coordinate environments of Ca^{2+}/Lu^{3+}, Zr^{4+} and Al^{3+} (b). The symbol * represents the peak due to ZrO_2.

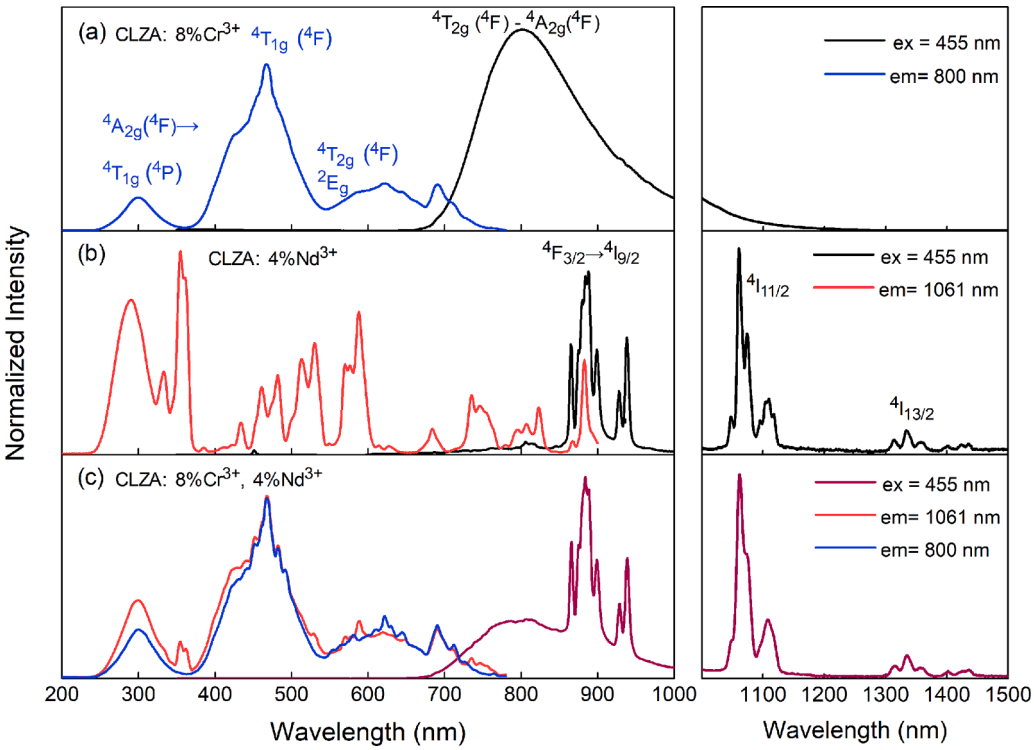

Fig. 2. Excitation and emission spectra of $Ca_2LuZr_2Al_3O_{12}$:8%Cr^{3+} (a), $Ca_2LuZr_2Al_3O_{12}$: 4%Nd^{3+} (b) and $Ca_2LuZr_2Al_3O_{12}$: 8%Cr^{3+}, 4%Nd^{3+} (c).

8%Cr, $Ca_2LuZr_2Al_3O_{12}$: 8%Cr, 4%Nd, $Ca_2LuZr_2Al_3O_{12}$: 1%Nd phosphors were shown in the Fig. S1. The excitation spectrum of Nd^{3+} emission at 1061 nm in $Ca_2LuZr_2Al_3O_{12}$: Cr^{3+}, Nd^{3+} is identical to that of $Ca_2LuZr_2Al_3O_{12}$:Cr^{3+}, indicating that Nd^{3+} is excited mainly by energy transfer from Cr^{3+} in $Ca_2LuZr_2Al_3O_{12}$: Cr^{3+}, Nd^{3+}. The energy level diagram of Cr^{3+} and Nd^{3+} with the energy transfer process is illustrated in Fig. S2.

The emission spectra of $Ca_2LuZr_2Al_3O_{12}$: 8%Cr^{3+}, $x$$Nd^{3+}$ (x= 0–10%), under 455 nm excitation, are shown in Fig. 3a. From the figure, the Nd^{3+} emission lines are rising and the Cr^{3+} emission bands are falling as the increasing of x. The IQEs of the total NIR emissions are

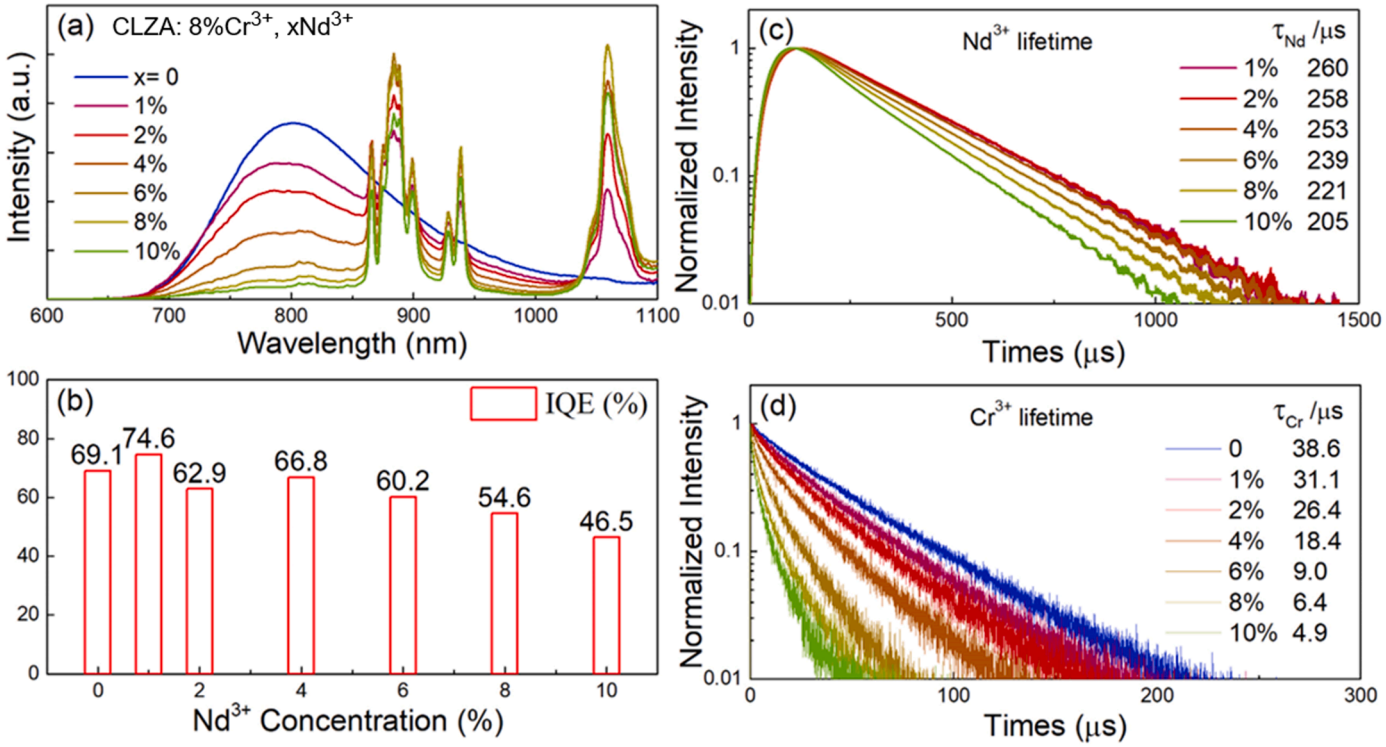

Fig. 3. Luminescent properties of $Ca_2LuZr_2Al_3O_{12}$:8%Cr^{3+}, $x$$Nd^{3+}$ (x = 0–10%): (a) Emission spectra under 455 nm excitation, (b) IQEs for different x, (c) Decay curves of Nd^{3+} emission and (d) Decay curves of Cr^{3+} emission after pulse excitation at 460 nm.

measured for different x, as shown in Fig. 3b, it can be found that there is an IQE enhancement from 69.1% to 74.6%, as the increasing of x from 0 to 1%. The result is the consequence of energy transfer from Cr^{3+} to the more efficient Nd^{3+} emitting center. The emission efficiency of Nd^{3+} can be calculated using the fluorescence lifetime and radiative lifetime of Nd^{3+}. The fluorescence lifetime of Nd^{3+} in $Ca_2LuZr_2Al_3O_{12}$: 8%Cr^{3+}, xNd^{3+} is 260 μs for $x = 1\%$, as shown in Fig. 3c. The radiative lifetime and the emission spectra of $Ca_2LuZr_2Al_3O_{12}$: 1%Nd^{3+} at 77 K were shown in Fig. S3 and Fig. S4. It can be seen that the radiative lifetime is close to the lifetime of $Ca_2LuZr_2Al_3O_{12}$: 1%Nd^{3+} at 77 K, which is measured to be 263 μs. Then, the quantum emission efficiency of Nd^{3+} in $Ca_2LuZr_2Al_3O_{12}$: 8%Cr^{3+}, 1%Nd^{3+} is calculated to be 98.9%, close to 1, which is indeed much higher than that (69.1%) of $Ca_2LuZr_2Al_3O_{12}$: 8% Cr^{3+}. Hence, the emission of Nd^{3+}, instead of Cr^{3+}, through energy transfer from Cr^{3+} will lead to the enhancement of overall IQE, which is attributed to the restriction of the non-radiation transition. In addition, the efficiency of energy transfer (η_{ET}), radiation (η_R) and non-radiation (η_{NR}) of Cr^{3+} at various Nd^{3+} concentrations are shown in Fig. S5. However, as doped concentration of Nd^{3+} is higher than 1%, the IQE is decreased, which is attributed to the waste of some excitation energies induced by increase of Nd^{3+}.

The efficiency of energy transfer can be calculated by the following equation, [36–39] which is based on the intensity decrease of Cr^{3+} emission (Fig. 3a) or lifetime shortening (Fig. 3d) of it, with the increase of x in $Ca_2LuZr_2Al_3O_{12}$: 8%Cr^{3+}, xNd^{3+}.

$$\eta_{ET} = 1 - I_{Cr}/I_{Cr_0} \tag{1}$$

$$\eta'_{ET} = 1 - \tau_{Cr}/\tau_{Cr_0} \tag{2}$$

Where I_{Cr} and I_{Cr_0} is Cr^{3+} emission intensity, τ_{Cr} and τ_{Cr_0} is Cr^{3+} emission lifetime in the presence of and in the absence of Nd^{3+}, respectively. The calculated values of energy transfer efficiency are very close, as shown in Fig. 4a. The average of the two efficiencies, $\overline{\eta}_{ET}$, is adopted in this paper. Based on the kinetic analysis of energy transfer, I_{Nd}/I_{Cr} can be expressed by

$$\frac{I_{Nd}}{I_{Cr}} = \frac{\overline{\eta}_{ET}\cdot\eta_{Nd}}{(1-\overline{\eta}_{ET})\cdot\eta cr_o} \tag{3}$$

Where I_{Nd} and I_{Cr} are emission intensity of $Nd^{3+}$and Cr^{3+}, η_{Nd} and η_{Cr_0} are the quantum efficiency of Nd^{3+} and Cr^{3+} at the absence of Nd^{3+}, respectively. Hence, a proportional relationship between $\eta_{Nd}\cdot\overline{\eta}_{ET}/(1-\overline{\eta}_{ET})$ and I_{Nd}/I_{Cr} can be observed, as shown in Fig. 4b. Meanwhile, Fig. 4c shows the dependence between $\overline{\eta}_{ET}/(1-\overline{\eta}_{ET})$ and x, and the slope is 1 for small x and 2 for higher x. This result is in good consistent with the Dexter's expression of energy transfer[40].

The mechanism of energy transfer is analysed based on the decay curve of Cr^{3+} emission using Inokuti-Hirayama formula: [37, 41]

$$I = I_0\exp\left[-\frac{4}{3}\pi\Gamma\left(1-\frac{3}{s}\right)N_a\alpha^{\frac{3}{s}}t^{\frac{3}{s}}\right] \tag{4}$$

Where I and I_0 are the decay curve of Cr^{3+} in the presence of and in the absence of Nd^{3+}, respectively. s is a coefficient with values of 6 (for dipole–dipole interactions), 8 (dipole–quadrupole interactions) and 10 (quadrupole-quadrupole interactions), respectively. N_a is the number of acceptor ions (Nd^{3+}) per unit volume Fig. 4.d-4i show a linear dependence between log*{-ln[I/I$_0$]}* and log*(t)*, with the slop of 3/*s*. Thus, *s* is close to 6, indicating the dipole–dipole interaction between Cr^{3+} and Nd^{3+} in energy transfer process.

3.3. Thermal stability

The emission spectra, at different temperatures, of $Ca_2LuZr_2Al_3O_{12}$: 8%Cr^{3+}, xNd^{3+} ($x = 0$, 1% and 8%) are depicted in Fig. S6 and Fig. 5. As shown, the quenching temperature increases from 450 K up to 550 K as the increasing of x, from 0 to 10%. On one hand, the quenching temperature increasing indicates that Nd^{3+} emission has a high thermal stability, compared with Cr^{3+}, which is in accordance with high IQE of Nd^{3+}. On the other hand, the thermal de-excitation of Cr^{3+} can be suppressed by energy transfer, as our previous study has shown. [29, 42-44]

3.4. Super-broadband NIR pc-LED

The $Ca_2LuZr_2Al_3O_{12}$: Cr^{3+}, Nd^{3+} converted NIR pc-LED is fabricated and its emission spectra, NIR output powers and power conversion efficiencies are measured at different drive currents, as shown in Fig. S7. The emission spectrum of the $Ca_2LuZr_2Al_3O_{12}$: Cr^{3+}, Nd^{3+} pc-LED appears a deep cavity around 1000 nm, which is not a good broadband NIR

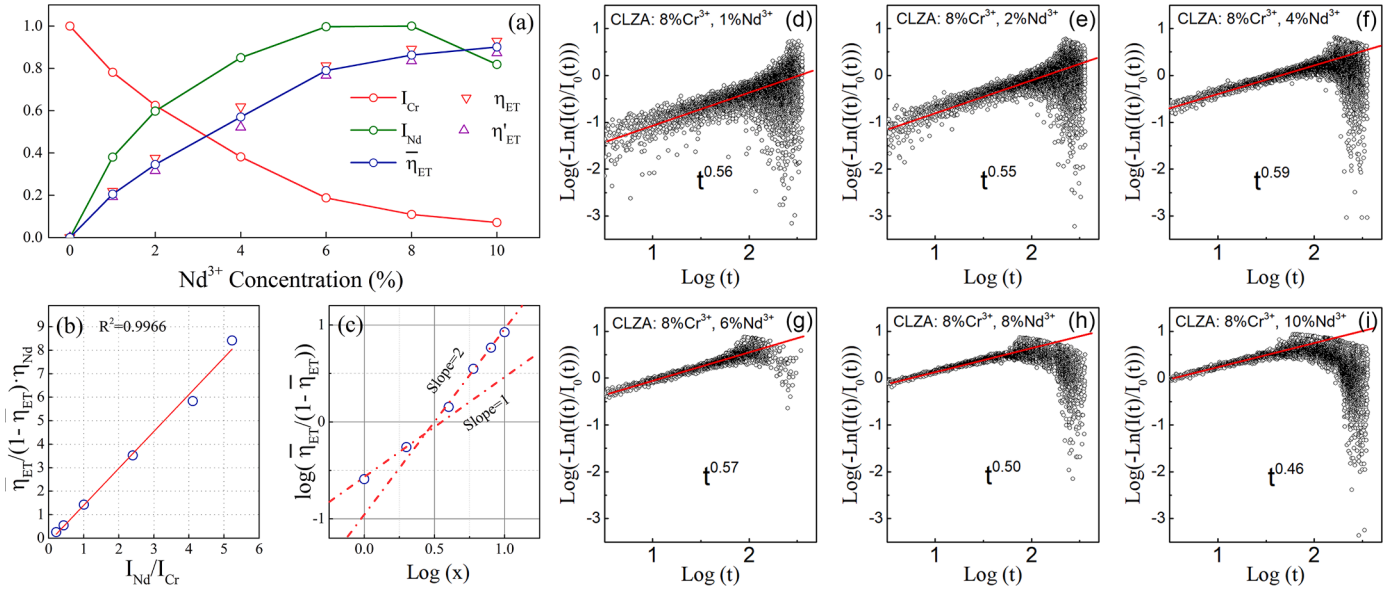

Fig. 4. (a) The *x* dependence of Cr^{3+}, Nd^{3+} emission intensity, energy transfer efficiencies calculated based on Cr^{3+} emission intensity, lifetimes, and the average of it. (b) The dependence of $\eta_{Nd}\overline{\eta}_{ET}/(1-\overline{\eta}_{ET})$ on luminescence intensity ratio I_{Nd}/I_{Cr}. (c) log(*x*) dependence on log($\overline{\eta}_{ET}/(1-\overline{\eta}_{ET})$). And (d-i) the relationship between Log*[-Ln(I(t)/I$_0$(t))]* and Log*(t)* of $Ca_2LuZr_2Al_3O_{12}$: 8%Cr^{3+}, xNd^{3+} ($x = 0.01$–0.10).

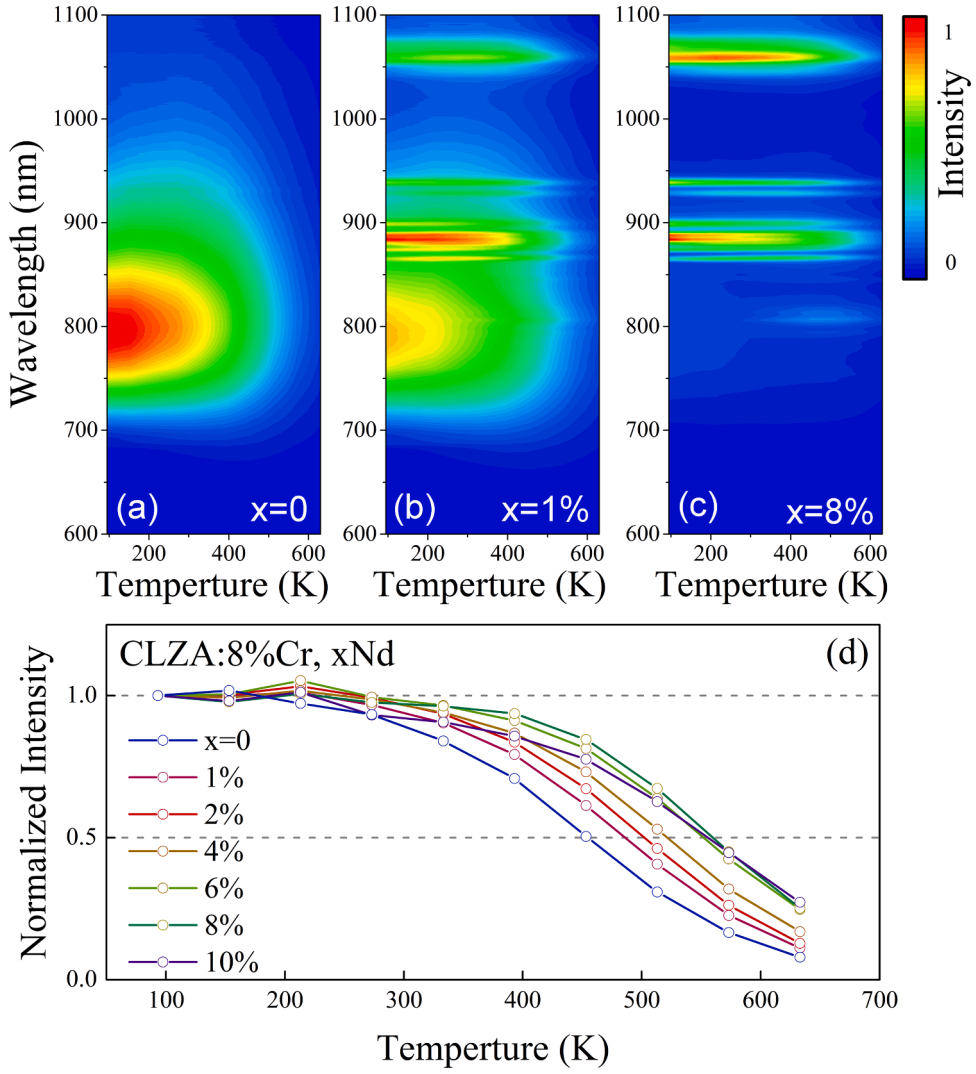

Fig. 5. Emission spectra at different temperatures for $x = 0$ (a), 1% (b) and 8% (c), and temperature dependence of the total emission intensity (d).

light source. To broaden the band with no obvious deficiency of spectral component within it, a NIR super-broadband pc-LED is fabricated, using the blend of $Ca_2LuZr_2Al_3O_{12}$: 8%Cr^{3+}, 2%Nd^{3+} and $Ca_2LuZr_2Al_3O_{12}$: 8% Cr^{3+}, 2%Yb^{3+} phosphors as fluorescence converter. The NIR emission spectra of the blend phosphor pc-LED (Fig. 6a) is just the superposition of $Ca_2LuZr_2Al_3O_{12}$: 8%Cr^{3+}, 2%Nd^{3+} emission (Fig. 6b) and $Ca_2LuZr_2Al_3O_{12}$: 8%Cr^{3+}, 2%Yb^{3+} emission (Fig. 6c), exhibiting improved spectral distribution compared to both of $Ca_2LuZr_2Al_3O_{12}$: Cr^{3+}, Nd^{3+} pc-LED (Fig. S7) and $Ca_2LuZr_2Al_3O_{12}$: Cr^{3+}, Yb^{3+} pc-LED [29]. The bandwidth is 350 nm, broader than that (320 nm) of $Ca_2LuZr_2Al_3O_{12}$: Cr^{3+}, Yb^{3+} pc-LED, [29] due to the appearance of the strong Nd^{3+} emission band at 1060 nm, and it is longer than the wavelength (1030 nm) of Yb^{3+} emission. The emission spectra of the pc-LED including a blue band, from LED chip, and a NIR emission band from the phosphor blend. The emission spectra enhance as the increase of drive current, while the spectral distribution sustains stable, as shown in Fig. 6a.

Fig. 6d manifests the dependence of electricity-to-NIR light conversion efficiency and the NIR light output power on drive current for the pc-LED. The conversion efficiency reaches 22.3% at 20 mA, with the NIR output power of 11.8 mW, 16.2% at 100 mA and the NIR light output power is 47.6 mW. The bandwidth and power conversion efficiency of the present pc-LED are improved, compared to the NIR pc-LEDs [29–31] ever reported at the same drive current. The decrease of electricity-to-NIR light conversion efficiency is caused by the well-known efficiency droop of blue LED chip rather than phosphor degradation.

4. Conclusion

Blue light excitable NIR $Ca_2LuZr_2Al_3O_{12}$: Cr^{3+}, Nd^{3+} phosphors are prepared by solid state reaction. From the emission spectra of the phosphors, we can see a band at 800 nm of Cr^{3+} emission and a group of Nd^{3+} emission bands, with quantum emission close to 100%, distributed in range of 850–1100 nm, excited by energy transfer from Cr^{3+} to Nd^{3+}. The IQE and thermal stability are both improved by adding Nd^{3+} in $Ca_2LuZr_2Al_3O_{12}$ Cr^{3+}, due to the energy transfer from Cr^{3+} to the more efficient Nd^{3+}. The IQE is promoted from 69.1% to 74.6% and the quenching temperature is increased from 450 K to 550 K. Energy transfer is governed by dipole–dipole interaction.

NIR super-broadband pc-LED is fabricated, and the blend of $Ca_2LuZr_2Al_3O_{12}$: 8%Cr^{3+}, 2%Nd^{3+} and $Ca_2LuZr_2Al_3O_{12}$: 8%Cr^{3+}, 2% Yb^{3+} phosphors are fluorescence converter. The NIR emission spectrum of the blend phosphor pc-LED exhibits improved spectral distribution, compared to both of $Ca_2LuZr_2Al_3O_{12}$: Cr^{3+}, Nd^{3+} pc-LED and $Ca_2LuZr_2Al_3O_{12}$: Cr^{3+}, Yb^{3+} pc-LED. The bandwidth reaches 350 nm, broader than that (320 nm) of $Ca_2LuZr_2Al_3O_{12}$: Cr^{3+}, Yb^{3+} pc-LED. The electricity-to-NIR light conversion efficiency of the blend phosphor pc-LED reaches 22.3%, at 20 mA drive current, with a NIR output power

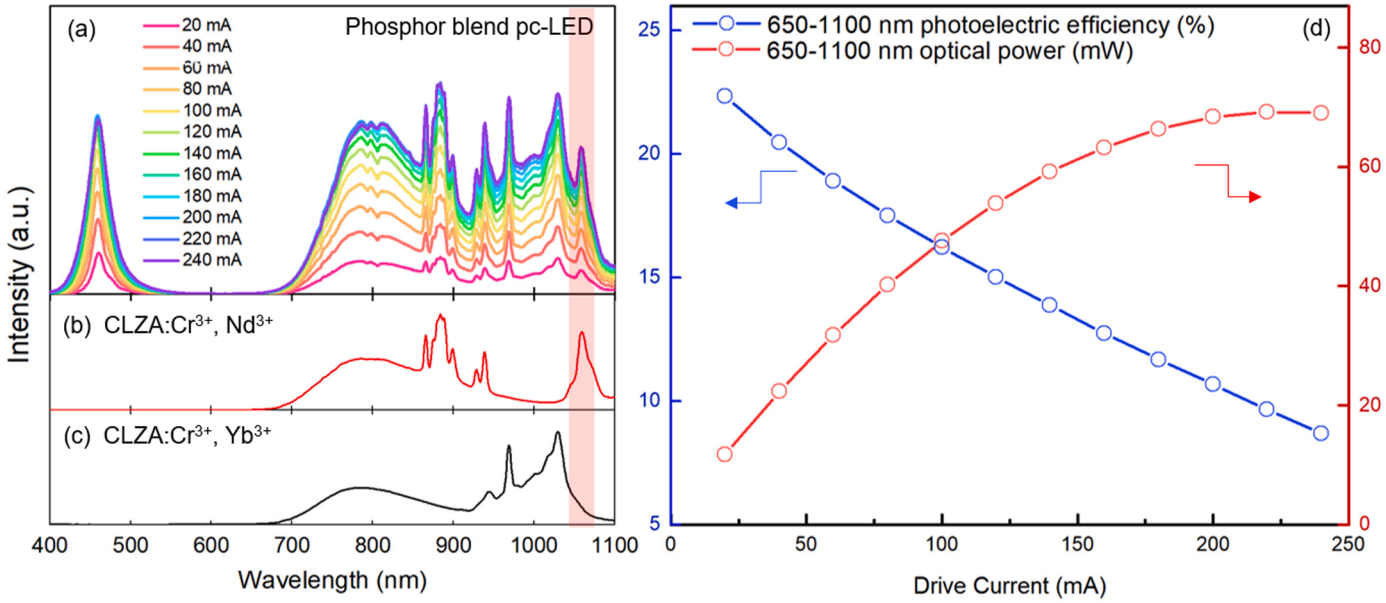

Fig. 6. Emission spectra of pc-LED under different drive currents (a), $Ca_2LuZr_2Al_3O_{12}$: 8%Cr^{3+}, 2%Nd^{3+} (b), $Ca_2LuZr_2Al_3O_{12}$: 8%Cr^{3+}, 2%Yb^{3+} (c). The light-red region represents the spectral extension to the longer wavelength due to appearance of Nd^{3+} emission band at 1060 nm. (d) Dependence of NIR output power and electricity-to-NIR light conversion efficiency on drive current for the pc-LED.

of 11.8 mW, 16.2% at 100 mA with the NIR light output power of 47.6 mW. The bandwidth and power conversion efficiency of the present pc-LED are improved, compared to the NIR pc-LEDs ever reported. Our researches suggest the great potential of $Ca_2LuZr_2Al_3O_{12}$: Cr^{3+}, Nd^{3+} phosphors for super broadband NIR pc-LEDs.

Declaration of Competing Interest

The authors declare that they have no known competing financial interests or personal relationships that could have appeared to influence the work reported in this paper.

Acknowledgments

This work is supported by National Natural Science Foundation of China (Grant No. 52072361, 12074373, 12074374, 51772286, 11974346, 11874055, 11904361), Youth Innovation Promotion Association CAS No. 2020222, Key Research and Development Program of Jilin province (20200401050GX, 20200401004GX and 20210201024GX). Cooperation project between Jilin Province and Chinese Academy of Sciences (2020SYHZ0013).

Supplementary materials

Supplementary material associated with this article can be found, in the online version, at doi:10.1016/j.materresbull.2022.111797.

References

[1] A.M.C. Davies, A. Grant, Review: near infra-red analysis of food, Int. J. Food Sci. Technol. 22 (1987) 191–207.
[2] E. Mehinagic, G. Royer, R. Symoneaux, D. Bertrand, Prediction of the sensory quality of apples by physical measurements, J. Frédérique, Postharvest Biol. Technol. 34 (2004) 257–269.
[3] W.T. Renfroe, S.J. Kays, Nondestructive spectrophotometric determination of dry matter in onions, J. Amer. Soc. Ilort. Sci. 110 (1985) 297–303.
[4] B. Zeng, Z. Huang, A. Singh, Y. Yao, A.K. Azad, A.D. Mohite, A.J. Taylor, D. R. Smith, H.T. Chen, Hybrid graphene metasurfaces for high-speed mid-infrared light modulation and single-pixel imaging, Light: Sci. Appl. 7 (2018) 523–530.
[5] A.T. Eggebrecht, S.L. Ferradal, A. Robichaux-Viehoever, M.S. Hassanpour, H. A. Dehghani, Z. Snyder, T. Hershey, J.P. Culver, Mapping distributed brain function and networks with diffuse optical tomography, Nature Photon 8 (2014) 448–454.
[6] D. Hayash, A.M. Dongen, J. Boerekamp, S. Spoor, G. Lucassen, J. Schleipen, A broadband LED source in visible to short-wave-infrared wavelengths for spectral tumor diagnostics, Appl. Phys. Lett. 110 (2017) 259, 247.
[7] Q.Y. Shao, H. Ding, L.Q. Yao, J.F. Xu, C. Liang, J.Q. Jiang, Photoluminescence properties of a $ScBO_3$: Cr^{3+} phosphor and its applications for broadband near-infrared LEDs, RSC Adv 8 (2018) 12035–12042.
[8] L.L. Zhang, D.D. Wang, Z.D. Hao, X. Zhang, G.H. Pan, H.J. Wu, J.H. Zhang, Cr^{3+}-doped broadband NIR garnet phosphor with enhanced luminescence and its application in NIR spectroscopy, Adv. Opt. Mater. 7 (2019), 1900185, 1-1900185.8.
[9] W.T. Huang, C.L. Cheng, B. Zhen, C.W. Yang, K.M. Lu, C.Y. Kang, C.M. Lin, R.S. Liu, Broadband Cr^{3+}, Sn^{4+}-doped oxide nanophosphors for infrared mini light-emitting diodes, Angew. Chem. Int. Ed. 58 (2019) 2069–2072.
[10] C. Chen, J. Wang, S. Bi, Y.L. Huang, H.J. Seo, Energy transfer and luminescence quenching of Cr^{3+}-doped $LiGaW_2O_8$, J. Alloys Compd. 786 (2019) 1051–1059.
[11] C.P. Wang, X.M. Wang, Y. Zhou, S. Zhang, H. Jiao, An ultra-broadband near infrared Cr^{3+}-activated gallogermanate $Mg_3Ga_2GeO_8$ phosphor as light sources for food analysis, ACS Appl. Electron. Mater. 1 (2019) 1046–1053.
[12] M. Back, Ueda J, M.G. Brik, T. Lesniewski, S. Tanabe, Revisiting Cr^{3+}-doped $Bi_2Ga_4O_9$ spectroscopy: crystal field effect and optical thermometric behavior of near-infrared-emitting singly-activated phosphors, ACS Appl. Mater. Interfaces 10 (2018) 41512–41524.
[13] B. Malysa, A. Meijerink, W.W. Wu, T. Jüstel, On the influence of calcium substitution to the optical properties of Cr^{3+} doped $SrSc_2O_4$, J. Lumin. 190 (2017) 234–241.
[14] D.D. Xu, Q. Zhang, X.M. Wu, W.W. Li, J.X. Meng, Synthesis, luminescence properties and energy transfer of Ca_2MgWO_6: Cr^{3+}, Yb^{3+} phosphors, Mater. Res. Bull. 110 (2019) 135–140.
[15] S.T. Lai, B.H.T. Chai, M. Long, M.D. Shinn, A new near-infrared tunable room temperature solid state laser La3Ga5SiO14: Cr3+, Adv. Solid State Lasers. Opt. Soc. Am. (1987) PD1.
[16] J. Luo, B.T. Wu, B. Zhu, S.F. Zhou, H.C. Yang, S. Ye, G. Lakshminarayana, J.R. Qiu, Energy transfer between Cr^{3+} and Ni^{2+} in transparent glass ceramics containing β-Ga_2O_3 nanocrystals, J. Appl. Phys. 106 (2009), 053527.
[17] B. Malysa, A. Meijerink, W. Wu, T. Jüstel, Temperature dependent Cr3+ photoluminescence in garnets of the type X3Sc2Ga3O12 (X= Lu, Y, Gd, La), J. Lumin. 190 (2017) 234–241.
[18] A. Zabiliūtė, S. Butkutė, A. Žukauskas, P. Vitta, A. Kareiva, Sol-gel synthesized far-red chromium-doped garnet phosphors for phosphor-conversion light-emitting diodes that meet the photomorphogenetic needs of plants, Appl. Opt. 53 (2014) 907–914.
[19] L.L. Zhang, S. Zhang, Z.D. Hao, X. Zhang, G.H. Pan, Y.S. Luo, H.J. Wu, J.H. Zhang, A high efficiency broad-band near-infrared $Ca_2LuZr_2Al_3O_{12}$: Cr^{3+} garnet phosphor for blue LED chips, J. Mater. Chem. C. 6 (2018) 4967–4976.
[20] H.T. Zeng, T.L. Zhou, L. Wang, R.J. Xie, Two-site occupation for exploring ultra-broadband near-infrared phosphor—double-perovskite La_2MgZrO_6: Cr^{3+}, Chem. Mater. 31 (2019) 5245–5253.

[21] Z.W. Jia, C.X. Yuan, Y.F. Liu, X.J. Wang, P. Sun, L. Wang, H.C. Jiang, J. Jiang, Strategies to approach high performance in Cr^{3+}-doped phosphors for high-power NIR-LED light sources, Light: Sci. Appl. 9 (2020).
[22] X.X. Xu, Q.Y. Shao, L.Q. Yao, Y. Dong, J.Q. Jiang, Highly efficient and thermally stable Cr^{3+}-activated silicate phosphors for broadband near-infrared LED applications, Chem. Eng. J. 383 (2019), 129108.
[23] M.T. Tran, D.Q. Trung, N. Tu, D.D. Anh, L.T.H. Thu, N.V. Du, N.V. Quang, N. T. Huyen, N.D.T. Kien, D.X. Viet, N.D. Hung, P.T. Huy, Single-phase far-red-emitting $ZnAl_2O_4:Cr^{3+}$ phosphor for application in plant growth LEDs, J. Alloys Compd. 884 (2021), 161077.
[24] J.W. Qiao, G.J. Zhou, Y.Y. Zhou, Q.Y. Zhang, Z.G. Xia, Divalent europium-doped near-infrared-emitting phosphor for light-emitting diodes, Nat. Commun. 10 (2019) 5267.
[25] V. Rajendran, M.H. Fang, G.N.D. Guzman, T. Lesniewski, S. Mahlik, M. Grinberg, G. Leniec, S.M. Kaczmarek, Y.S. Lin, K.M. Lu, C.M. Lin, H. Chang, S.F. Hu, R.S. Liu, Super broadband near-infrared phosphors with high radiant flux as future light sources for spectroscopy applications, ACS Energy Lett. 3 (2018) 2679–2684.
[26] L.Q. Yao, Q.Y. Shao, X.X. Xu, Y. Dong, C. Liang, J.H. He, J.Q. Jiang, Broadband emission of single-phase $Ca_3Sc_2Si_3O_{12}$: Cr^{3+}/Ln^{3+} (Ln = Nd, Yb, Ce) phosphors for novel solid-state light sources with visible to near-infrared light output, Ceram. Int. 45 (2019) 14249–14255.
[27] L.Q. Yao, Q.Y. Shao, S.Y. Han, C. Liang, J.H. He, J.Q. Jiang, Enhancing Near-Infrared photoluminescence intensity and spectral properties in Yb^{3+} codoped $LiScP_2O_7:Cr^{3+}$, Chem. Mater. 32 (2020) 2430–2439.
[28] E.T. Basore, H. Wu. W. G. Xiao, G.J. Zheng, X.F. Liu, J.R. Qiu, High-power broadband NIR LEDs enabled by highly efficient blue-to-NIR conversion, Adv. Opt. Mater. 9 (2021), 2001660.
[29] S. He, L.L. Zhang, H. Wu, H.J. Wu, G.H. Pan, Z.D. Hao, X. Zhang, L.G. Zhang, H. Zhang, J.H. Zhang, Efficient super broadband NIR $Ca_2LuZr_2Al_3O_{12}:Cr^{3+}$, Yb^{3+} garnet phosphor for pc-LED light source toward NIR spectroscopy applications, Adv. Opt. Mater. 8 (2020), 1901684.
[30] D. Li, D. Han, S.N. Qu, L. Liu, P.T. Jing, D. Zhou, W.Y. Ji, X.Y. Wang, T.F. Zhang, D. Z. Shen, Supra-(carbon nanodots) with a strong visible to near-infrared absorption band and efficient photothermal conversion, Light: Sci. Appl. 5 (2016) e16120.
[31] R.J. Xie, Light-emitting diodes: brighter NIR-emitting phosphor making light sources smarter, Light: Sci. Appl. 9 (2020) 155.
[32] Y. Zorenko, V. Gorbenko, Growth peculiarities of the R3Al5O12 (R= Lu, Yb, Tb, Eu–Y) single crystalline film phosphors by liquid phase epitaxy, Radiat. Measure. 42 (2007) 907–910.
[33] S.K. Ranjan, A.K. Soni, V.K. Rai, Nd3+-Yb3+/Nd3+-Yb3+-Li+ co-doped Gd2O3 phosphors for up and down conversion luminescence, Lumin 33 (2018) 647–653.
[34] B. Klimesz, G.D. Dzik, R. Lisiecki, W.R. Romanowski, Systematic study of spectroscopic properties and thermal stability of lead germanate glass doped with rare-earth ions, J. Non-Cryst. Solids 354 (2008) 515–520.
[35] A.A. Kaminskii, G. Boulon, M. Buoncristiani, B. Di Bartolo, A. Kornienko, V. Mironov, Spectroscopy of a new laser garnet $Lu_3Sc_2Ga_3O_{12}$: Nd^{3+}. Intensity luminescence characteristics, stimulated emission, and full set of squared reduced-matrix elements$|<\| U (t)\|>|2$ for Nd^{3+} ions, Phys. Status Solidi A. 141 (1994) 471–494.
[36] P.I. Paulose, G. Jose, V. Thomas, N.V. Unnikrishnan, M.K.R. Warrier, Sensitized fluorescence of Ce^{3+}/Mn^{2+} system in phosphate glass, J. Phys. Chem. Solids 64 (2003) 841–846.
[37] M. Inokuti, F. Hirayama, Influence of energy transfer by the exchange mechanism on donor luminescence, J. Chem. Phys. 43 (1965) 1978–1989.
[38] Y.H. Song, E.K. Ji, B.W. Jeong, M.K. Jung, E.Y. Kim, D.H. Yoon, High-power laser-driven ceramic phosphor plate for outstanding efficient white light conversion in application of automotive lighting, Sci. Rep. 6 (2016) 31206.
[39] G. Blasse, Energy transfer in oxidic phosphors, Philips Res. Rep. 24 (1969) 131.
[40] D.L. Dexter, J.H. Schulman, Theory of concentration quenching in inorganic phosphors, J. Chem. Phys. 22 (1954) 1063–1070.
[41] L.L. Zhang, J.H. Zhang, G.H. Pan, X. Zhang, Z.D. Hao, Y.S. Luo, H.J. Wu, Low-concentration Eu^{2+}-doped $SrAlSi_4N_7$: Ce^{3+} yellow phosphor for wLEDs with improved color-rendering index, Inorg. Chem. 55 (2016) 9736–9741.
[42] Y. Xiao, Z.D. Hao, L.L. Zhang, X. Zhang, G.H. Pan, H.J. Wu, Y.S. Luo, J.H. Zhang, An efficient green phosphor of Ce^{3+} and Tb^{3+}-codoped $Ba_2Lu_5B_5O_{17}$ and a model for elucidating the high thermal stability of the green emission, J. Mater. Chem. C. 6 (2018) 5984–5991.
[43] Y. Xiao, Z.D. Hao, L.L. Zhang, W.G. Xiao, D. Wu, X. Zhang, G.H. Pan, Y.S. Luo, J. H. Zhang, Highly efficient green-emitting phosphors $Ba_2Y_5B_5O_{17}$ with low thermal quenching due to fast energy transfer from Ce^{3+} to Tb^{3+}, Inorg. Chem. 56 (2017) 4538–4544.
[44] J.H. Zhang, Z.D. Hao, J. Li, X. Zhang, Y.S. Luo, G.H. Pan, Observation of efficient population of the red-emitting state from the green state by non-multiphonon relaxation in the Er^{3+}-Yb^{3+} system, Light: Sci. Appl. 4 (2015) e239.